Proceedings of the 17th World Congress
The International Federation of Automatic Control
Seoul, Korea, July 6-11, 2008

Uniformity Control in Planetary Chemical Vapor Deposition Reactor Systems

Raymond A. Adomaitis *

* *Department of Chemical and Biomolecular Engineering, Institute for Systems Research, University of Maryland, College Park, MD, 20742 USA (Tel: 301-405-2969; e-mail: adomaiti@umd.edu).*

Abstract: A simplified model of the spatially dependent deposition profile in chemical vapor deposition reactors with planetary wafer rotation is developed. The model focuses on reactors operated in "depletion" mode, a situation where the precursor species have undergone a sequence of gas-phase decomposition reactions leaving only the deposition species to diffuse to and react on the substrate surface, generating the thin film. The model is used to identify the reactor design and operating parameters that influence the shape of the deposition profile. By projecting the deposition profile onto the rotating wafers, the thickness uniformity as a function of reactor system operating parameters also is examined.

Keywords: Applications in semiconductor manufacturing; Control of distributed systems; Process modeling and identification.

1. INTRODUCTION

Chemical vapor deposition (CVD) reactors for thin-film semiconductor processing come in a variety of configurations, the choice of the design being driven by precursor physical properties, whether gas-phase reactions or the suppression of particle formation are important, and whether single or multi-wafer capabilities are necessary. As one example, consider the multi-wafer planetary reactor system shown in Fig. 1, a reactor used for epitaxial growth of a wide range of compound semiconductors. In this design, reactant gas flows radially outward from a central feed point over the susceptor containing the wafers, each of which rotates on its individual axis. This design has the effect of eliminating reactor-induced angular non-uniformity generators through susceptor rotation, and wafer rotation is used to reduce the intrinsic effect of gas phase reactant decomposition and precursor depletion in the gas phase.

From the first description of the planetary reactor system developed by Frijlink [1988], numerous simulation studies (including Frijlink [1988]) have been published describing the use of physically based models to identify operating conditions leading to relatively uniform films under wafer rotation. Typically, these studies include detailed, two-dimensional steady-state models of reactor heat transfer, reactant gas flow and chemical species reaction and transport. For example, starting chronologically from Frijlink [1988], Bergunde, et al. [1995] compared simulator predictions to experimentally measured film growth profiles and studied the effects of total gas flow and temperature on film growth. Jurgensen [1996] used a two-dimensional model of gas phase transport to study NH_3 gas phase decomposition in the production of GaN films. Bergunde, et al. [1997a] and Bergunde, et al. [1997b] developed highly detailed model elements describing heat transfer in planetary reactor systems, with emphasis on radiative heat transfer. Beccard, et al. [1999] used a 2D simulator to examine gas phase gallium precursor decomposition in GaN film growth and SiC film sensitivity to carrier gas flow rate. Dauelsberg, et al. [2000] used a simulator to study gas phase reaction mechanisms relevant to $Ga_{1-x}In_xP$ film growth. Karpov [2003] describes a highly detailed reactor model that includes particle formation mechanisms. Parikh and Adomaitis [2006] developed detailed simulators for GaN and later for uniformity control of SiC film growth (Parikh, et al [2007]). Most recently, Brien [2007] studied

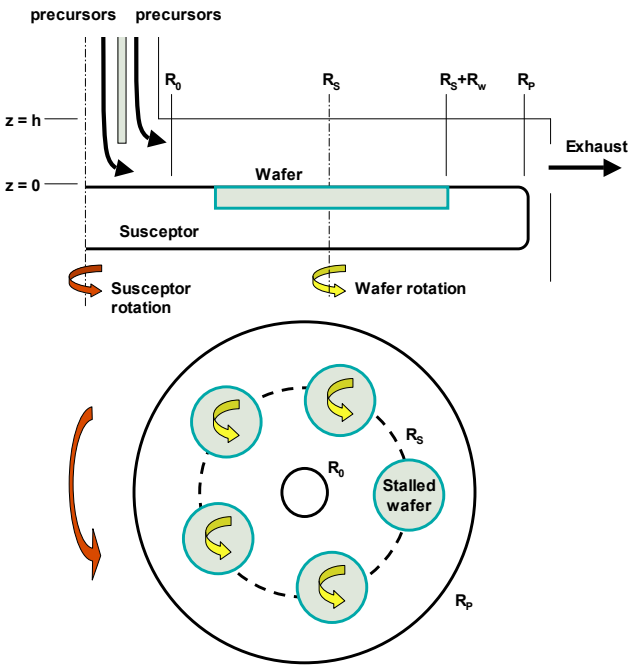

Fig. 1. Side (upper) and top (lower) views of a 5-wafer planetary reactor system.

GaAs film growth with a focus on reactor inlet design for uniformity control and effective precursor utilization.

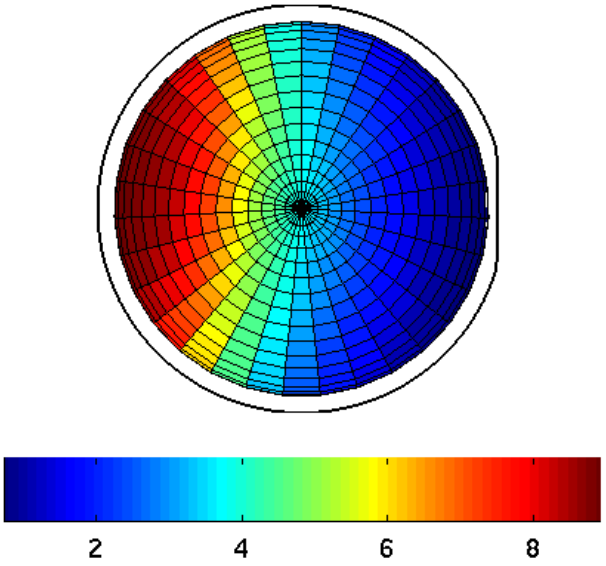

Fig. 2. *SiC film thickness (in μm) over a stalled wafer; reactant gas flow is from left to right. Experimental data are taken from Parikh, et al [2007].*

1.1 Depletion mode of operation

In all the modeling and optimization studies cited, one or more of the precursors undergoes a sequence of gas-phase decomposition reactions producing gas phase species capable of deposition. For example, in SiC deposition, silane undergoes the decomposition sequence

$$SiH_4 \rightarrow SiH_2 \rightarrow Si$$

where the atomic Si is primarily responsible for film formation. Likewise in GaN systems, trimethylgallium (TMG) thermally decomposes into the dimethyl- and monomethyl subalkyls in the following manner

$$TMG \rightarrow DMG \rightarrow MMG \rightarrow Ga.$$

with the MMG and atomic gallium contributing largely to the film growth rate (Parikh and Adomaitis [2006]).

Given these decomposition and deposition reaction pathways, the radial flow CVD reactor can be conceptually split up into three distinct regions of reactor operation along the radial direction r: the first is the central region where the reactants heat quickly (see Parikh and Adomaitis [2006] for an example) due to the high reactor temperature required for epitaxial growth. After sufficient heating, the gas phase reactions commence, and the second reactor region is characterized by an increasing deposition rate with respect to r. The third and final region begins after the peak deposition rate; in this region, the species involved in gas phase reactions have been depleted and only those important to film growth remain, resulting in a radial deposition profile that tapers off with increasing r. See Fig. 2 for an example of thickness data on a stalled wafer, illustrating how a relatively thick film is formed at the wafer leading edge and the nearly order of magnitude drop in thickness in the direction of gas flow, a film profile characteristic of the depletion zone.

1.2 Uniformity control in the depletion zone

In virtually all of the optimization studies cited, the reactor operating parameters were set so that the wafer was located in the depletion zone. Therefore, we examine the following four issues defining the main contributions of this paper:

(1) Develop a simplified model of the deposition rate profile in the depletion zone;
(2) Identify which design and operating parameters affect the deposition profile in this zone to determine which parameters are most effective for controlling non-uniformity;
(3) Determine the range of the parameters where reasonable uniformity (e.g., less than 1% mean squared non-unifomity) is to be found;
(4) Examine representative published results to determine if the simplified reactor model and uniformity optimization results are consistent with the previous studies.

2. REACTOR MODELING

In the depletion zone of the reactor, no gas phase reactions take place and the reactor temperature can be assumed constant. We also assume pressure-induced density variations are negligible, and viscosity, density, and all other gas properties are constant with respect to spatial position in this reaction zone.

We define the flux of a gas phase species s_i in the r direction

$$\text{flux} = c_i v_r - D_i \frac{\partial c_i}{\partial r}$$

where c_i is the concentration of species i, v_r the radial velocity, and D_i the diffusivity of species i, a material balance on a two-dimensional differential element gives

$$\frac{1}{r}\frac{\partial}{\partial r}\left(x_i r v_r - D_i r \frac{\partial x_i}{\partial r}\right) + \frac{\partial}{\partial z}\left(x_i v_z - D_i \frac{\partial x_i}{\partial z}\right) = 0 \quad (1)$$

where x_i is the mole fraction of species i. For constant density ρ and viscosity μ, the equations of fluid motion can be written as

$$\rho\left(v_r\frac{\partial v_r}{\partial r} + v_z\frac{\partial v_r}{\partial z}\right) = -\frac{\partial p}{\partial r} + \mu\left[\frac{1}{r}\frac{\partial}{\partial r}\left(r\frac{\partial v_r}{\partial r}\right) + \frac{\partial^2 v_r}{\partial z^2} - \frac{v_r}{r^2}\right]$$

$$\rho\left(v_r\frac{\partial v_z}{\partial r} + v_z\frac{\partial v_z}{\partial z}\right) = -\frac{\partial p}{\partial z} + \mu\left[\frac{1}{r}\frac{\partial}{\partial r}\left(r\frac{\partial v_z}{\partial r}\right) + \frac{\partial^2 v_z}{\partial z^2}\right]$$

together with the continuity equation:

$$\frac{1}{r}\frac{\partial}{\partial r}(r v_r) + \frac{\partial v_z}{\partial z} = 0$$

where $p(r,z)$ is the gas pressure and v_z the vertical component of gas velocity.

2.1 Simplifications

Assuming the gas flow field is fully developed, that the ceiling height h is constant with respect to the radial coordinate r, and that the fluid inertial terms are negligible (ρ is small), $v_z = 0$ and the fluid flow modeling equations reduce to the single equation

$$0 = -\frac{\partial p}{\partial r} + \mu\left[\frac{1}{r}\frac{\partial}{\partial r}\left(r\frac{\partial v_r}{\partial r}\right) + \frac{\partial^2 v_r}{\partial z^2} - \frac{v_r}{r^2}\right]$$

which can be further simplified using the continuity equation

$$\frac{1}{r}\frac{\partial}{\partial r}(rv_r) = 0$$

to find

$$\mu\frac{\partial^2 v_r}{\partial z^2} = \frac{\partial p}{\partial r}$$

which can be solved for $v_r(r,z)$ given the boundary conditions $v_r(r,0) = v_r(r,h) = 0$ and that the total volumetric flow of reactant gas V at reactor operating temperature and pressure:

$$v_r(r,z) = -z(h-z)\frac{1}{2\mu}\frac{\partial p}{\partial r} = z(h-z)\frac{3V}{\pi h^3 r}.$$

For

$$x_i r v_r \gg D_i r\frac{\partial x_i}{\partial r}$$

and $v_z = 0$, equation (1) reduces to the well-known Graetz problem Hsu [1963]:

$$z(h-z)\frac{3V}{\pi h^3}\frac{1}{r}\frac{\partial x_i}{\partial r} = D_i\frac{\partial^2 x_i}{\partial z^2}$$

subject to boundary conditions

$$x_i(R_0, z) = 1 \text{ for } z \in (0,h)$$
$$x_i(r,0) = x_i(r,h) = 0 \qquad r \in [R_0, R_P].$$

See Fig. 1 and Table 1 for the definitions of R_0, R_W, R_P and other notation.

Defining

$$\eta = \frac{r - R_0}{R_S + R_W - R_0} \qquad \text{and} \qquad \zeta = \frac{z}{h}$$

and the Peclet number and dimensionless inlet position parameter η_0 for this system as

$$P_e = \frac{3Vh}{\pi D_i(R_S + R_W - R_0)^2}, \qquad \eta_0 = \frac{R_0}{R_W + R_S - R_0}$$

we find

$$\zeta(1-\zeta)\frac{1}{\eta+\eta_0}\frac{\partial x}{\partial \eta} = \frac{1}{P_e}\frac{\partial^2 x}{\partial \zeta^2} \tag{2}$$

subject to

$$x_i(0,\zeta) = 1 \text{ for } \zeta \in (0,1) \tag{3}$$
$$x_i(\eta,0) = x_i(\eta,1) = 0 \qquad \eta \in [0,1]. \tag{4}$$

At this point, we make the following observation: the deposition profile depends *only* on two parameters: η_0 and P_e. Physically, this translates into a clear definition of the operational parameters that most influence the film thickness profile: the carrier gas flow rate V can be used to adjust P_e which is proportional to V. While the starting point of the depletion zone η_0 will also depend on V, η_0 can be manipulated by the feed gas heating rate or susceptor temperature.

2.2 Solution

Equation 2, subject to the boundary conditions (3-4), can be solved using the eigenfunction expansion general solution

$$x(\eta,\zeta) = \sum_{i=1}^{\infty} a_i e^{\lambda_i(\eta+\eta_0)^2/2P_e}\psi_i(\zeta)$$

where the $\psi_i(\eta)$ are orthonormal eigenfunctions (with respect to inner product weight function $\zeta(1-\zeta)$) computed as solutions to the eigenvalue problem

$$\frac{d^2\psi}{d\zeta^2} = \lambda\psi\zeta(1-\zeta) \qquad \text{subject to } \psi(0) = \psi(1) = 0.$$

The inlet condition is used to find the particular solution

$$e^{\lambda_i\eta_0^2/2P_e}a_i = \int_0^1 \psi_i(\zeta)\,\zeta(1-\zeta)d\zeta.$$

This solution procedure works well for large P_e and small η_0; however, for small values of P_e and when $\eta > 0$, the solution converges slowly, if at all, because the a_i grow infinitely large with increasing i. Therefore, we pose a solution in the form

$$x(\eta,\zeta) = \sum_{j=1}^{J_0} a_j\psi_j(\zeta) + \sum_{i=1}^{I}\sum_{j=1}^{J} b_{i,j}\phi_i(\eta)\psi_j(\zeta) \tag{5}$$

where the $\psi_j(\eta)$ are the even, normalized solutions to the eigenvalue problem

$$\frac{d^2\psi}{d\zeta^2} = \lambda\psi \qquad \text{subject to } \psi(0) = \psi(1) = 0$$

and the $\phi_i(\eta)$ are orthonormal polynomials in η that vanish at $\eta = 0$. Evaluating (5) at $\eta = 0$ and projecting the result onto each basis function gives

$$a_j = \sigma_j\int_0^1 \psi_j(\zeta)d\zeta, \qquad j = 1,\ldots,J_0$$

where the σ_j are Fourier-space filter coefficients used to reduce the Gibbs' oscillations at the reaction zone inlet. A Galerkin procedure then is implemented by substituting (5) into (2) and projecting the residual onto each basis function to find

$$\sum_{i=1}^{I}\sum_{j=1}^{J} b_{i,j}\left\langle\frac{\zeta(1-\zeta)}{\eta+\eta_0}\phi_i'\psi_j, \phi_m\psi_n\right\rangle = \frac{1}{P_e}a_n\lambda_n + \frac{1}{P_e}b_{m,n}\lambda_n$$

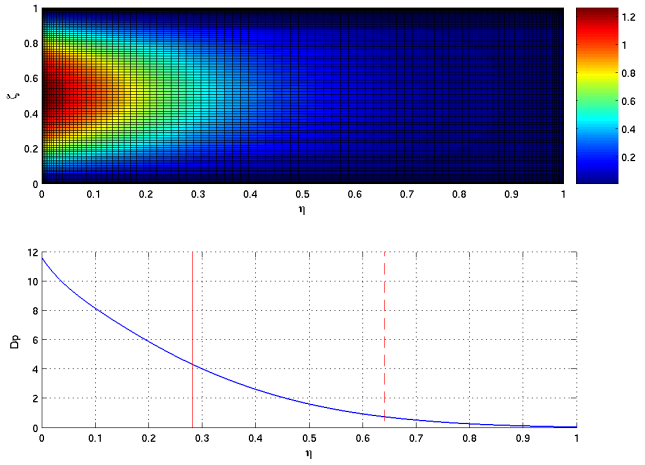

Fig. 3. Representative gas-phase concentration plot for $P_e = 9$ (top); resulting deposition profile as a function of reactor position (bottom). Red line indicates wafer leading edge location, dashed red line indicates wafer centerline. Simulation results correspond to parameters listed in Table 1.

2.3 Representative simulation

Consider a representative planetary reactor system with the design and operating parameters listed in Table 1. These design and operating parameter values correspond to the work of Beccard, et al. [1999], where an SiC film deposition process was simulated over a 2in wafer. The value of $P_e = 9$ was determined so that our simulation results would corroborate with the lowest-flow simulation of Beccard, et al. [1999].

In the upper plot of Fig. 3, gas flows from left to right between the upper and lower walls of the reaction chamber. When the gas enters, it is most highly concentrated in the deposition species; this concentration rapidly diminishes to near zero at the reactor outlet ($\eta = 1$) because of the diffusion to and deposition on both reactor walls.

2.4 Deposition rate

Because of the high susceptor temperature typically used in epitaxial MOCVD, the reactor operates in a mass transfer-limited mode - this fact was used to define the zero-concentration boundary conditions of the Graetz problem. Under these conditions, the deposition rate $D_p(\eta)$ at the reactor roof and along the length of the susceptor is

$$D_p(\eta) = D_d c_T \frac{\partial x_d(\eta)}{\partial z}\bigg|_{z=0,h}$$

Parameter	Value
R_0	0.0349 m
R_w	0.0251 m
R_s	0.0797 m
P_e	9
I	8
J	10
J_0	2

Table 1. Representative reactor operating, design, and simulation parameters.

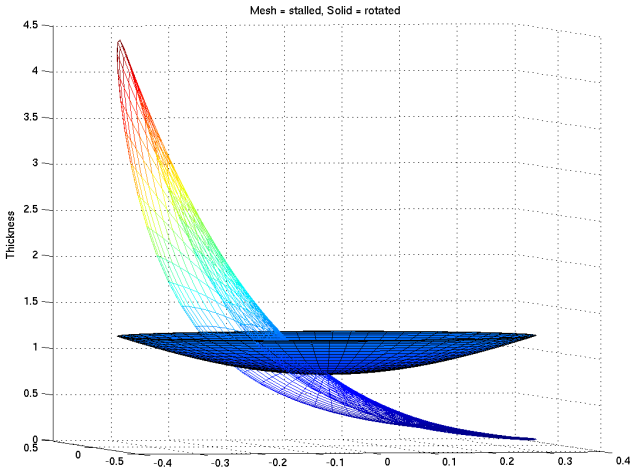

Fig. 4. Stalled (mesh) and rotationally averaged (solid) wafer maps for $P_e = 9$

$$= \frac{D_d c_T}{h} \frac{\partial x_d(\eta)}{\partial \zeta}\bigg|_{\zeta=0,1}$$

where the subscript d denotes the gas phase species that contribute to the deposition process. See the lower plot of Fig. 3 for a representative deposition profile over the susceptor surface.

We project this deposition profile over the wafer domain to find $\delta(r', \theta)$, where r' and θ denote coordinates local to the wafer. An example of what such a projection may look like can be seen in Fig. 4 where the mesh surface illustrates the deposition profile over the stalled wafer and the deposition profile D_p corresponds to the simulation results illustrated in Fig. 3. The rotationally averaged profiles are found to be

$$\alpha(r') = \frac{1}{2\pi} \int_0^{2\pi} \delta(r', \theta)\, d\theta.$$

This bowl-shaped rotationally averaged profile is shown as the solid curve in Fig. 4.

2.5 Comparison to detailed simulations

Consider Fig. 5, where one SiC film thickness profile taken from Beccard, et al. [1999] is shown as the thicker solid curve; this profile corresponds the lowest carrier gas flow rate of Fig. 4 of the cited study. We plot our solutions found for values of $P_e = [2, 9, 50, 500]$, demonstrating the excellent match achieved between the deposition profiles for the case $P_e = 9$. The changes in the deposition profile with P_e also match those found in Beccard, et al. [1999]. Overall, we find that our simplified model does an excellent job of approximating a more detailed reactor system model.

2.6 Non-uniformity control

If the average film thickness over the entire wafer surface is given by

$$\alpha_{avg} = \frac{1}{\pi R_w^2} \int_0^{R_w} \alpha(r')\, r\, dr$$

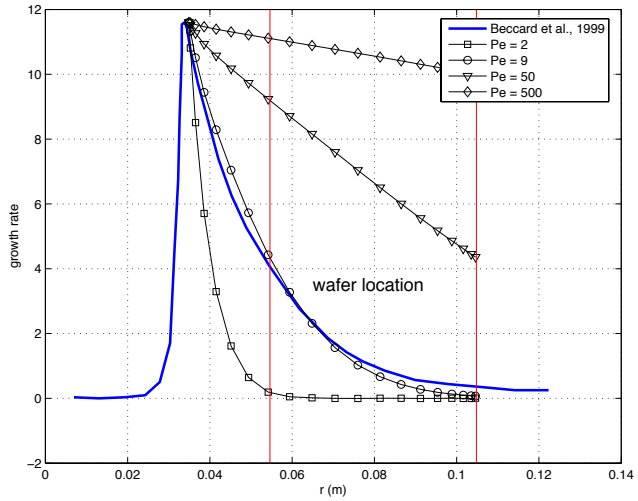

Fig. 5. Depletion plot with data estimated from Beccard, et al. [1999]. Growth rate is given in arbitrary units in the cited study.

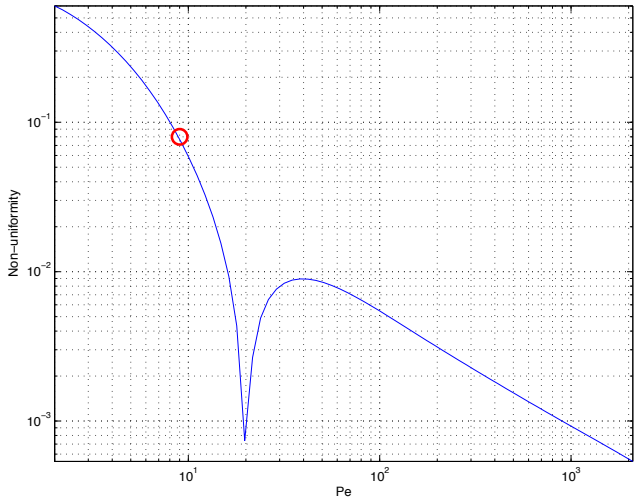

Fig. 6. Wafer uniformity N_u as a function of P_e. Red circle marks the point where $P_e = 9$ and the nonuniformity is approximately 8%.

we assess the degree of nonunifomity as

$$N_u = \|(\delta(r', \theta)/\alpha_{avg} - 1\|.$$

Simulation results in Beccard, et al. [1999] demonstrated little change in η_0 as the carrier gas flow rate was varied; therefore, P_e can be adjusted independently of η_0 in that system, making N_u a function only of P_e. In this plot we see that for all $P_e > 15$ we achieve less than 1% non-uniformity over the rotationally averaged wafer. There is a local non-uniformity minimum at approximately $P_e = 20$, and the non-uniformity approaches zero as $P_e \to \infty$, the case where the carrier gas flow rate is so high that the film becomes uniform over the stalled wafer surface. While this condition can produce perfect thickness uniformity, it comes as great expense because of the excessive consumption of reactant gases, making the local minimum an attractive alternative setpoint.

ACKNOWLEDGEMENTS

The author gratefully acknowledges the support of the National Science Foundation through grant CTS-0554045

REFERENCES

Beccard, R., D. Schmitz, E. G. Woelk, G. Strauch, Y. Makarov, M. Heuken, M. Deschler, and H. Juergensen (1999) High temperature CVD systems to grow GaN or SiC based structures, *J. Mat. Sci. and Eng.* B61-62 314-319.

Bergunde, T., D. Gutsche, L. Kadinski, Yu. Makarov, and M. Weyers (1995) Transport and reaction behavior in Aix-2000 Planetary metalorganic vapor phase epitaxy reactor, *J. Crystal Growth* **146** 564-569.

Bergunde, T., M. Dauelsberg, L. Kadinski, Yu. N. Makarov, M. Weyers, D. Schmitz, G. Strauch, and J. Jurgensen (1997) Heat transfer and mass transport in a multiwafer MOVPE reactor: modelling and experimental studies, *J. Crystal Growth* **170** 66-71.

Bergunde, T., M. Dauelsberg, L. Kadinski, Yu. N. Makarov, V. S. Yuferev, D. Schmitz, G. Strauch, and J. Jurgensen (1997) Process optimization of MOVPE growth by numerical modelling of transport phenomena including thermal radiation, *J. Crystal Growth* **180** 660-669.

Brien, D., M. Dauelsberg, K. Christiansen, J. Hofeldt, M. Deufel, and M. Heuken (2007) Modelling and simulation of MOVPE of GaAs-based compound semiconductors in production scale Planetary Reactors, *J. Crystal Growth* **303** 330-333.

Dauelsberg, M., L. Kadinski, Yu. N. Makarov, T. Bergunde, G. Strauch, and M. Weyers (2000) Modeling and experimental verification of transport and deposition behavior during MOVPE of $Ga_{1-x}In_xP$ in the Planetary Reactor, *J. Crystal Growth* **208** 85-92.

Frijlink, P. M. (1988) A new versatile, large size MOVPE reactor, *J. Crystal Growth* **93** 207-215.

Hsu, S. T. (1963) *Engineering Heat Transfer*, D. Van Nostrand Company, Inc.

Jurgensen, H., D. Schmitz, G. Strauch, E. Woelk, M. Dauelsberg, L. Kadinski, Yu. N. Makarov (1996) MOCVD equipment for recent developments towards the blue and green solid state laser *MRS Internet J. Nitride Semicond. Res.* **1**, Article 26.

Karpov, S. Yu. (2003) Advances in the modeling of MOVPE processes, *J. Crystal Growth* **248** 1-7.

Parikh, R. P. and R. A. Adomaitis (2006) An overview of gallium nitride growth chemistry and its effect on reactor design: Application to a planetary radial flow CVD system, *J. Crystal Growth* **286** 259-278.

Parikh, R. P., R. A. Adomaitis, J. D. Oliver, and B. H. Ponczak (2007) Implementation of a geometrically-based criterion for film uniformity control in a planetary SiC CVD reactor system, *J. Process Control* **17** 477-488.